

Recognizing the Important Role of Surface Barriers in MOR Zeolite Catalyzed DME Carbonylation Reaction

Kaipeng Cao, Dong Fan, Mingbin Gao, Benhan Fan, Nan Chen, Linying Wang, Peng Tian,* and Zhongmin Liu*



Cite This: *ACS Catal.* 2022, 12, 1–7



Read Online

ACCESS |



Metrics & More



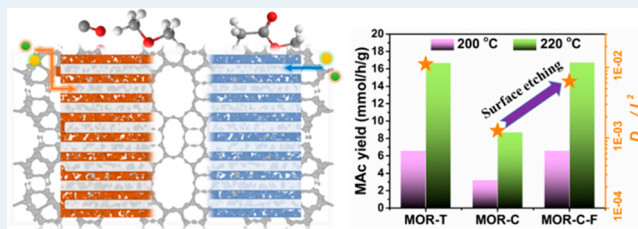
Article Recommendations



Supporting Information

ABSTRACT: Transport resistance in microporous zeolites has an important impact on their applications in catalysis. Relative to the well-known intracrystalline transport resistance, the significance of surface barriers on the catalytic performance of zeolites has not been well recognized. Herein, we report that the DME carbonylation reaction can be governed by surface barriers on zeolites, affecting both the catalyst activity and stability. The two MOR zeolites used for the investigation were synthesized by different organic structure-directing agents (OSDAs). They possess similar Si/Al ratios, diffusion lengths, Al distributions, and acidities but quite different diffusion properties. The MOR-C sample with severe transport limitations exhibits inferior apparent activity ($\sim 50\%$ lower) and poor stability in comparison compared with the MOR-T sample. Chemical etching of the outer layer of as-made MOR-C crystals has been proven to be an effective strategy to reduce surface barriers, enhance mass transport properties, and improve the activity and stability of the MOR catalyst. The carbonylation activity of etched MOR-C is indeed comparable to that of MOR-T. This work highlights the importance of controlling the synthetic strategy and surface barriers on zeolite crystals for the design/development of highly efficient catalysts.

KEYWORDS: MOR zeolite, surface barriers, mass transfer, DME carbonylation



Zeolites are important inorganic microporous materials, which have wide applications in chemical industries as highly efficient catalysts and adsorbents. Due to their uniform porosity of molecular dimensions, zeolites exhibit prominent performance as shape-selective catalysts.¹ However, the confined channels of zeolites inevitably bring about severe diffusion limitations for guest molecules.^{2–7} Intracrystalline diffusion resistance has been acknowledged as an important factor influencing the zeolite-catalyzed reactions. Great efforts have been dedicated to predicting the intracrystalline diffusivities and to reducing the internal transport resistance.^{8–11} In addition, the importance of surface resistance on mass transport is also receiving increasing attention. By using microimaging techniques to monitor the uptake of molecules in SAPO-34 crystal, it was revealed that surface barriers may govern the mass transport process, and their contribution to the overall transport resistance depends on the guest molecules under investigation.¹² Moreover, recent results show that surface barriers obviously increase in hierarchical or nanosized zeolites and become an important factor affecting the transport process, due to the change in surface properties (surface defects, pore narrowing, or blocking).^{13,14}

The essential role of surface barriers in mass transfer suggests its importance for zeolite-catalyzed reactions. However, the knowledge about the impact of surface barriers on catalysis is limited, and only a few zeolites (ZSM-5,¹⁵

SAPO-34,^{16,17} and Pt/Beta¹⁸) are involved. Given that the qualities of zeolites have been demonstrated to be heavily dependent on the synthetic strategy, recognizing the relation between synthesis and zeolite properties should be more critical for controlling the surface barriers and the catalyst performance. This knowledge is also expected to benefit the rational design and development of zeolite catalysts.

MOR zeolite is an important member of the zeolite family, which has attracted considerable attention in recent years due to its excellent activity and ultrahigh product selectivity in dimethyl ether (DME) carbonylation and syngas/methanol to ethylene.^{19–23} The DME carbonylation process catalyzed by the zeolite was industrialized in 2017, which opens a new route for ethanol generation from coal and natural gas.²⁴ It has been revealed that the Brønsted acid sites located in the confined side pockets of MOR zeolite are the unique active centers for the DME carbonylation reaction, whereas the 12-membered ring (12-MR) pore provides a mass transfer channel for both reactants and products.^{25–27} In order to improve the activity

Received: October 29, 2021

Revised: November 30, 2021

Published: December 9, 2021



and stability of MOR catalyst, many strategies have been developed, including pyridine modification,²⁸ acid/alkali post-treatment,^{29,30} and the synthesis of nanosized MOR zeolite.^{31–35} The first strategy can help avoid side reactions by poisoning the acid sites in 12-MR, while the last two aim to reduce the intracrystalline diffusion resistance. However, the importance of surface barriers on this reaction has not yet received attention as far as we know, even though they may play a critical role in determining the catalyst performance.

In the present study, we report for the first time that surface diffusion barriers over MOR zeolites can dominate the mass transfer process and significantly affect the DME carbonylation performance. Two MOR zeolites with similar Si/Al ratios were synthesized using different OSDAs. The MOR zeolite synthesized hydrothermally by tetraethylammonium hydroxide (TEAOH) and trimethylamine (TMA) was denoted MOR-T, while the sample synthesized using cyclohexylamine (CHA) was denoted MOR-C. The texture, acidity, diffusion properties, and catalytic performance of the zeolites were investigated in detail, and the important role of surface barriers on the catalytic performance was elucidated.

Figure 1 displays the structural and morphological properties of the two samples synthesized using different OSDAs. The

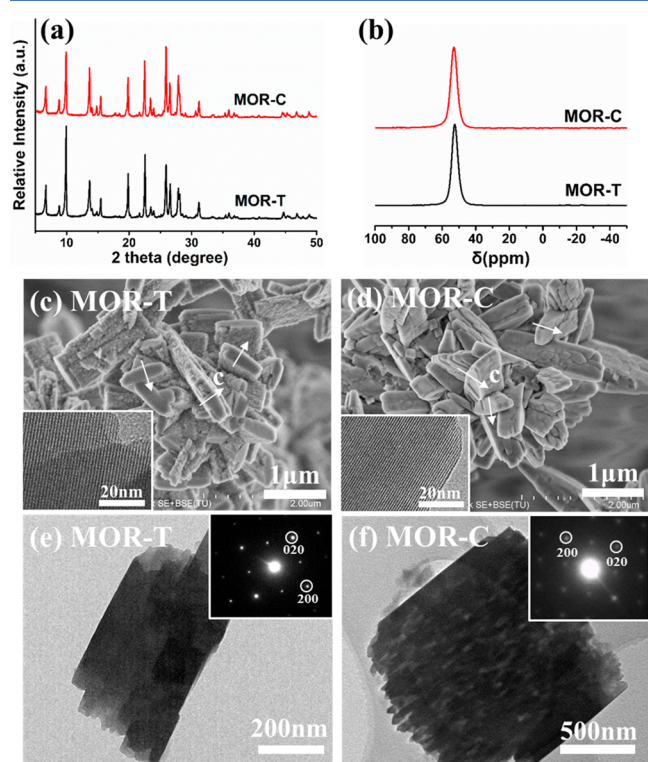


Figure 1. Structure and morphology of the as-made MOR samples: (a) XRD patterns; (b) ^{27}Al MAS NMR spectra; (c, d) representative SEM and HRTEM images (the arrows in the figures illustrate the direction of 12-MR channels); (e, f) SAED patterns viewed along the c -axis direction.

XRD patterns (Figure 1a) present the characteristic peaks of a typical MOR type structure for MOR-T and MOR-C, both of which have similar peak intensities. The SEM images in Figure 1c,d show that MOR-T crystals have a platelike morphology with a rough surface, while MOR-C has a relatively smooth surface. The corresponding HRTEM images (the insets) evidence that both samples are single crystals with good

crystallinity. The SAED patterns in Figure 1e,f reveal that the shortest dimension of the crystals runs along the c -axis direction for either sample, with 12-MR channel lengths of less than 500 nm. The nitrogen adsorption/desorption isotherms of both samples in Figure S1 could be regarded as type I isotherms, implying negligible mesoporosity. The corresponding textural information is given in Table S2. The micropore volumes and micropore surface areas of MOR-T are larger than those of MOR-C, but the difference is not significant. Thermogravimetric analysis (TG) profiles in Figure S2 indicate that the weight losses of as-synthesized MOR-T and MOR-C are 7.8 and 6.0 wt % respectively, suggesting that MOR-T has a higher filling degree of micropores by organic amines.

The Si/Al ratios of the as-made MOR zeolites are presented in Table S2. Both samples possess similar bulk Si/Al ratios (derived from XRF), being 13.4 and 13.6 for MOR-T and MOR-C, respectively. Their surface Si/Al ratios, calculated to be 14.5 and 15.3 on the basis of the XPS results, show only slight deviations from the bulk ratios, indicating the relatively uniform Al distribution for both samples. The ^{27}Al MAS NMR spectra in Figure 1b show only one peak around 54 ppm, characteristic of tetraordinated Al species, suggesting that all of the Al atoms are in the framework.³⁶ On the basis of the ^{29}Si NMR spectra (Figure S3), the amounts of Si species of the two samples are close to each other, which implies similar arrangements of Al atoms. In addition, Co^{2+} exchange was carried out to learn the amount of Al pairs (Al–Si–Al and Al–Si–Si–Al) in the samples. Exchange degrees (Co^{2+}/Al) of 0.33 and 0.30 were obtained for MOR-T and MOR-C, respectively, suggesting their similar Al pair contents.^{37,38}

The acid properties of the protonated MOR samples are presented in Table S3 and Figure 2. NH_3 -TPD results (Figure 2a) show that the total acid amounts of MOR-T and MOR-C range from 0.85 to 0.86 mmol/g, and the NH_3 desorption peaks are centered at proximate temperatures, which implies the similar acid strengths of the samples. An ^1H MAS NMR

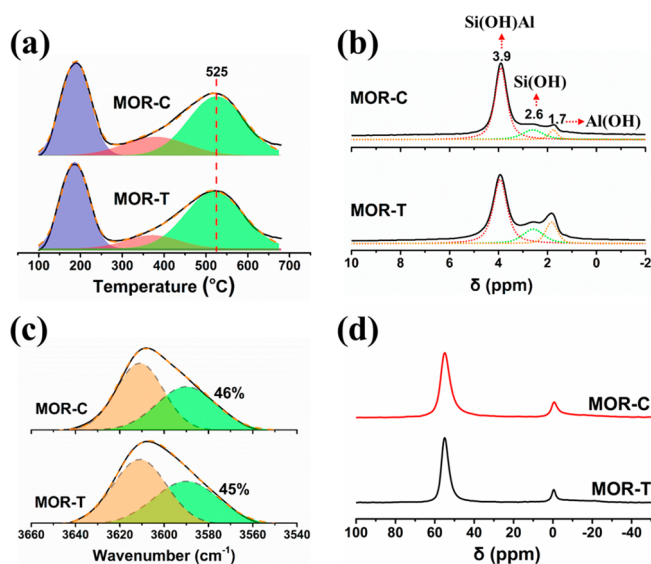


Figure 2. Acidity and Al coordination environments of the protonated MOR samples: (a) NH_3 -TPD profiles; (b) ^1H MAS NMR spectra; (c) FTIR spectra and deconvoluted bands corresponding to the acid sites in 12-MR channels (left) and 8-MR side pockets (right); (d) ^{27}Al MAS NMR spectra (as-made samples). The values in (c) refer to the proportion of the acid sites in 8-MR side pockets.

analysis was further carried out to quantify the Brønsted acid sites of the H-MOR samples (Figure 2b). On the basis of the deconvoluted results of ^1H NMR spectra (Table S2), the amounts of BASs are calculated to be 0.64 and 0.57 mmol/g for MOR-T and MOR-C, respectively. Moreover, the distribution of BASs in 12-MR and 8-MR channels, which is an important factor affecting the catalytic performance, was also investigated by FTIR and analyzed by a previously reported deconvolution method.^{39,40} According to the deconvolution results of the bridging hydroxyl group (Figure 2c), the proportions of BASs located in the 8-MR side pocket of MOR-T and MOR-C are 45% and 46%, respectively. The above characterization results clearly demonstrate that the MOR-T and MOR-C samples possess similar textural properties, Al distributions, and acid properties.

It has been recognized that the acid sites in the 12-MR main channels of zeolite MOR are prone to side reactions (DME to hydrocarbons) due to the lack of a space confinement effect, resulting in rapid carbon deposition and deactivation of the catalysts.^{27,41} Pyridine adsorption has been demonstrated to be an effective strategy for covering the acid sites in 12-MR channels, suppressing the side reactions, and improving the reaction stability and MAc selectivity in DME carbonylation.^{28,42} Thus, the catalytic performances of the samples were investigated herein with pyridine-modified H-MOR catalysts. As indicated in Figure 3a, both MOR-T and MOR-

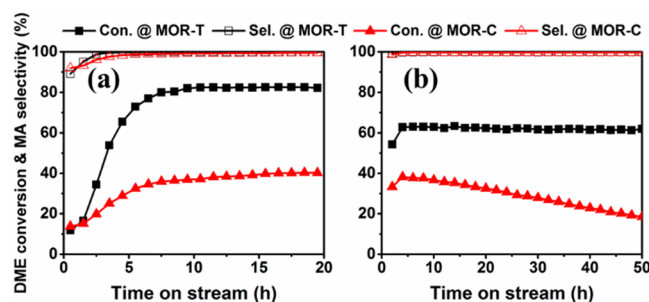


Figure 3. DME carbonylation performance over pyridine-modified H-MOR catalysts. Reaction conditions: (a) GHSV = 3600 mL/(g h), 200 °C, 2 MPa; (b) GHSV = 12000 mL/(g h), 220 °C, 2 MPa.

C show no obvious deactivation at 200 °C during a 20 h reaction, whereas DME conversion on MOR-T (82%) is about twice that on MOR-C (40%). When the reaction temperature is increased to 220 °C (Figure 3b), distinct variations of both the stability and activity can be observed for the two catalysts. Apart from the well-preserved catalytic stability (no obvious deactivation in 50 h), MOR-T also exhibits a higher DME conversion of about 63% at a GHSV value of 12000 mL/(g h). In sharp contrast, catalyst MOR-C shows inferior conversion with worse catalyst stability. The DME conversion decreased from 39% to 18% after a 50 h reaction. On consideration of the similar structural, textural, and acid properties of the two samples, it is speculated that the difference in reaction performance may result from their mass transfer properties.

The mass transfer properties of pyridine-modified MOR zeolites were first investigated by an intelligent gravimetric analyzer (IGA). MAc, the predominant product of the DME carbonylation reaction, was selected as the probe molecule for IGA measurement. As shown in Figure 4a, the MAc uptake rate is obviously faster in MOR-T than in MOR-C. Quantitative analyses of the diffusion properties of the samples

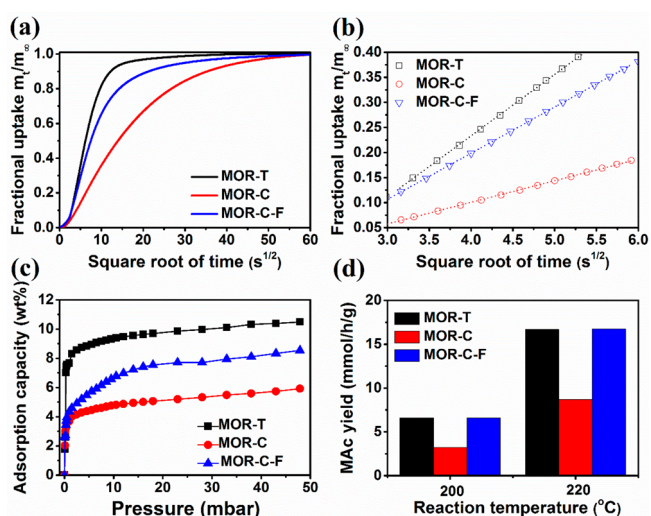


Figure 4. (a) MAc uptake rate inside pyridine-modified H-MOR. (b) Initial uptake rate. The symbols and dashed lines respectively represent the experimental data and fitting results by eq 4 in the Supporting Information. (c) Toluene adsorption isotherms for H-MOR. (d) MAc space–time yields on the pyridine-modified H-MOR catalysts (calculated on the basis of DME conversion and MAc selectivity at TOS = 20 h).

were further carried out based on Fick's second law (eq 4 in the Supporting Information). The fitting results of m_t/m_∞ versus $t^{1/2}$ show a good linearity (Figure 4b), and the values of the diffusion time constant (D_{eff}/L^2), good indicators of the mass transfer properties, could be evaluated from the slopes.^{43–45} The calculated D_{eff}/L^2 value is 1.12×10^{-2} for MOR-T and 1.26×10^{-3} for MOR-C. In consideration of similar 12-MR channel lengths of the two samples, the much lower uptake rate observed for MOR-C suggests the existence of severe diffusion barriers.

The TG curves of the two pyridine-modified catalysts are illustrated in Figure S4. The occluded pyridine is calculated to be 5.9 and 4.9 wt % for MOR-T and MOR-C, respectively. Clearly, the density difference of adsorbed pyridine in the 12-MR channels cannot account for the distinct mass transfer properties of the samples. Also, the possibility of an acidity-induced variation of the mass transfer properties has been excluded, as the two samples show high resemblance in their acid properties (acid quantity, strength, and distribution). In addition, although extraframework aluminol (EFAL) indeed exists in both H-MOR samples (Figure 2d), their relative quantities are quite similar, as revealed by the deconvoluted analysis of ^1H MAS NMR spectra (Figure 2b and Table S4). Thus, the different diffusion properties of the samples should stem from their intrinsic pore characteristics, rather than the acid site distribution/density, the influence of adsorbed pyridine molecules, the presence of EFAL, etc. To verify this speculation, toluene was used as a probe molecule to study the accessible volume of the samples (H-form). The toluene uptake isotherms are illustrated in Figure 4c. MOR-T exhibits a much higher accessible volume, whose toluene adsorption capacity is about 95% higher than that of MOR-C at 10 mbar ($P/P_0 \approx 0.2$).

To further figure out whether the diffusion barriers stem from the interior or the surface of the crystals, chemical etching using an acetone–HF acid solution was carried out to remove the outer layer of the as-made MOR-C crystals.^{46,47} The

corresponding sample was denoted as MOR-C-F, and its structural, textural, and acid properties were examined in detail. The XRD pattern (Figure S5) manifests typical diffraction peaks of the MOR-type structure. The SEM image (Figure S6) depicts no clear morphology changes after surface treatment. ²⁹Si MAS NMR spectra (Figure S3) evidence Si coordination environments of MOR-C-F similar to those of MOR-C, and no EFAL can be observed in the ²⁷Al spectrum (Figure S7). The Si/Al ratios in Table S2 show that both the bulk and surface composition of MOR-C-F is close to those of the parent sample. In addition, the N₂ sorption results (Figure S1 and Table S2) indicate that MOR-C-F has almost the same textural properties as its precursor. On the basis of NH₃-TPD and FTIR spectra (Figure S8), the acid amount and acid distribution of MOR-C-F are also revealed to be similar to those of MOR-C (Table S3). The above characterizations evidence that the interior of MOR-C-F crystals remains intact after the etching treatment.

Nevertheless, the diffusion resistance on MOR-C-F was significantly ameliorated in comparison with that on MOR-C (Figure 4a–c), as evidenced by the sharply enhanced MAC uptake rate ($D_{\text{eff}}/L^2 = 6.36 \times 10^{-3}$) and toluene sorption capacity. In addition, to quantitatively compare the variation of surface permeability (α) and intracrystalline diffusivity (D) on MOR-C and MOR-C-F, the IGA curves of *n*-butane uptake were further measured, and the data were fitted on the basis of a dual-resistance model (DRM).^{16,17} From Figure S9, similar intracrystalline diffusivity can be observed for both samples, in accordance with their similar textural properties discussed above. However, there is a significant difference in the surface permeability. The α value of MOR-C-F is much higher than that of MOR-C. These results demonstrate that the acetone–HF solution preferentially etches the crystal surface of the as-made MOR zeolite.

The carbonylation performances of MOR-C-F (pyridine-modified catalyst) are illustrated in Figure S10. The corresponding MAC yields of the samples are given in Figure 4d. An obviously improved carbonylation activity could be observed for the MOR-C-F sample after HF etching, with a MAC yield approaching that of MOR-T. Moreover, the catalytic stability of MOR-C-F at 220 °C is also clearly enhanced in comparison to that of MOR-C. It is noted that etching MOR-T by the same procedure as for MOR-C (sample MOR-T-F, Figures S5, S6, and S11) did not show promoting effect on its DME carbonylation performance, suggesting the better structural integrity of the surface of MOR-T crystals.

To check if the surface barriers have a general effect in catalysis, two more acid-catalyzed reactions (isopropylbenzene cracking and *n*-octane cracking) have been tested, and the corresponding results are shown in Figure S12. Clearly, the apparent activities of the catalysts in the two cracking reactions have the same sequence as that in the DME carbonylation reaction, confirming the high surface barriers on MOR-C.

To investigate the origin of surface barriers on MOR-C, acid treatment and alkali treatment were first explored to etch the as-made crystals. From Figure S13, both acid and alkali treatments cannot deliver a product with an enhanced conversion comparable to that of the HF-etched sample. Given that the acid treatment mainly etches Al species, alkali treatment removes Si species, and HF treatment etches Si and Al without bias,^{46,47} herein the weak effect of acid and alkali treatments on the improvement of activity implies that local disordered –Si–O–Al– connection (neither silica species nor

alumina species) at the shell of crystals may be responsible for the blocking/narrowing of the channels.

The effect of gel parameters on the synthetic products was also studied to understand the formation of surface barriers. As given in Tables S5–S8, the TEOH + TMA system has a much wider synthetic phase region in comparison to the CHA system for MOR synthesis. The CHA system has narrow product Si/Al ratios and is sensitive to the decreased gel alkalinity, OSDA, and Na₂O amounts. The crystallization processes of the two systems were further examined. The results are displayed in Figures S14 and S15. Both samples possess a rough surface at the early crystallization stage (12 h). After 16 h, the crystal surface of MOR-C becomes smooth, while the surface of MOR-T remains rough even after 24 h. It has been reported that quaternary ammonium cation TEA⁺ could adsorb on a certain crystal plane of zeolites and reduce the surface energy.^{48–50} Herein, the existence of TEA⁺ in the MOR-T system may contribute to the maintenance of the rough surface. On the other hand, given that the alkalinity and cation concentration (such as Na⁺) change significantly at different crystallization stages,^{51–53} and the phase region for CHA-templated MOR zeolite is much narrower, it is speculated that the variations of the gel environment may exert great influence toward the growth of MOR-C crystals at the latter stage of crystallization (with the formation of a smooth layer), causing the development of local structural disorder and consequently surface barriers for diffusion.

The DME carbonylation performances of the products synthesized under different conditions using CHA as the OSDA are shown in Figure S16. It can be found that changes in the gel alkalinity, product Si/Al ratio, H₂O/Si ratio, and crystallization time have less of an effect on the catalytic activity (40–56%), which implies that the varied synthetic conditions are helpless for the modification of surface diffusion resistance on MOR-C sample. According to these results, we speculated that the OSDAs employed for the synthesis are crucial for the quality of MOR products.

In conclusion, the DME carbonylation performance of two MOR zeolites was investigated to reveal the significant impact of surface barriers on the catalyst activity and stability. In comparison with the highly efficient catalyst MOR-T, MOR-C with severe surface barriers exhibits low catalytic activity and stability. Chemical etching using an acetone–HF solution is evidenced to be an effective route to reduce surface resistance, improve the apparent diffusivity of guest molecules, and enhance the carbonylation activity (comparable to that of MOR-T) and stability of the catalyst. Furthermore, it is found that the severe surface resistance on MOR-C may originate from a local disordered connection at the shell of crystals, and the OSDAs employed for the synthesis are crucial for the quality of MOR products. This study demonstrates that, in addition to acid properties and diffusion length, the control of surface barriers is essential for an improvement in the mass transfer and catalytic performance of zeolite catalysts.

■ ASSOCIATED CONTENT

Supporting Information

The Supporting Information is available free of charge at <https://pubs.acs.org/doi/10.1021/acscatal.1c04966>.

Gel compositions for the synthesis of MOR zeolites, deconvolution results of ¹H MAS NMR spectra, N₂ adsorption–desorption isotherms, thermal analysis

profiles of the as-made MOR samples and pyridine-modified H-MOR samples, ^{29}Si and ^{27}Al MAS NMR spectra, XRD patterns and SEM images of the samples, acidity of the H^+ -form MOR-C-F sample, DME carbonylation performances over pyridine-modified H^+ -form MOR catalysts and cracking reactions over H^+ -form MOR catalysts, and IGA curves of *n*-butane on H-MOR samples and the corresponding fitting results (PDF)

AUTHOR INFORMATION

Corresponding Authors

Peng Tian – National Engineering Laboratory for Methanol to Olefins, Dalian National Laboratory for Clean Energy, Dalian Institute of Chemical Physics, Chinese Academy of Sciences, Dalian 116023, People's Republic of China; Email: tianpeng@dicp.ac.cn

Zhongmin Liu – National Engineering Laboratory for Methanol to Olefins, Dalian National Laboratory for Clean Energy, Dalian Institute of Chemical Physics, Chinese Academy of Sciences, Dalian 116023, People's Republic of China; orcid.org/0000-0002-7999-2940; Email: liuzm@dicp.ac.cn

Authors

Kaipeng Cao – National Engineering Laboratory for Methanol to Olefins, Dalian National Laboratory for Clean Energy, Dalian Institute of Chemical Physics, Chinese Academy of Sciences, Dalian 116023, People's Republic of China; University of Chinese Academy of Sciences, Chinese Academy of Sciences, Beijing 100049, People's Republic of China

Dong Fan – National Engineering Laboratory for Methanol to Olefins, Dalian National Laboratory for Clean Energy, Dalian Institute of Chemical Physics, Chinese Academy of Sciences, Dalian 116023, People's Republic of China

Mingbin Gao – National Engineering Laboratory for Methanol to Olefins, Dalian National Laboratory for Clean Energy, Dalian Institute of Chemical Physics, Chinese Academy of Sciences, Dalian 116023, People's Republic of China; orcid.org/0000-0002-7143-2658

Benhan Fan – National Engineering Laboratory for Methanol to Olefins, Dalian National Laboratory for Clean Energy, Dalian Institute of Chemical Physics, Chinese Academy of Sciences, Dalian 116023, People's Republic of China; University of Chinese Academy of Sciences, Chinese Academy of Sciences, Beijing 100049, People's Republic of China

Nan Chen – National Engineering Laboratory for Methanol to Olefins, Dalian National Laboratory for Clean Energy, Dalian Institute of Chemical Physics, Chinese Academy of Sciences, Dalian 116023, People's Republic of China; University of Chinese Academy of Sciences, Chinese Academy of Sciences, Beijing 100049, People's Republic of China

Linying Wang – National Engineering Laboratory for Methanol to Olefins, Dalian National Laboratory for Clean Energy, Dalian Institute of Chemical Physics, Chinese Academy of Sciences, Dalian 116023, People's Republic of China

Complete contact information is available at:
<https://pubs.acs.org/10.1021/acscatal.1c04966>

Notes

The authors declare no competing financial interest.

ACKNOWLEDGMENTS

This work was supported by the Key Research Program of Frontier Sciences, Chinese Academy of Sciences (Grant No. QYZDB-SSW-JSC040), the National Natural Science Foundation of China (Nos. 21676262, 21991090, and 21991091), and funding from the French-Sino International Laboratory (LIA “Zeolites”).

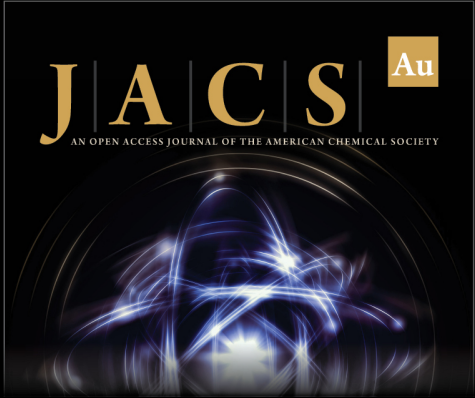
REFERENCES

- (1) Moliner, M.; Martinez, C.; Corma, A. Multipore Zeolites: Synthesis and Catalytic Applications. *Angew. Chem., Int. Ed.* **2015**, *54*, 3560–3579.
- (2) Peng, P.; Gao, X.-H.; Yan, Z.-F.; Mintova, S. Diffusion and catalyst efficiency in hierarchical zeolite catalysts. *Natl. Sci. Rev.* **2020**, *7*, 1726–1742.
- (3) Caro, J.; Noack, M.; Richtermendau, J.; Marlow, F.; Petersohn, D.; Griepentrog, M.; Kornatowski, J. Selective Sorption Uptake Kinetics Of N-hexane On Zsm-5 - A New Method For Measuring Anisotropic Diffusivities. *J. Phys. Chem.* **1993**, *97*, 13685–13690.
- (4) van Donk, S.; Bitter, J. H.; Verberckmoes, A.; Versluijs-Helder, M.; Broersma, A.; de Jong, K. P. Physicochemical characterization of porous materials: Spatially resolved accessibility of zeolite crystals. *Angew. Chem., Int. Ed.* **2005**, *44*, 1360–1363.
- (5) Losch, P.; Pinar, A. B.; Willinger, M. G.; Soukup, K.; Chavan, S.; Vincent, B.; Pale, P.; Louis, B. H-ZSM-5 zeolite model crystals: Structure-diffusion-activity relationship in methanol-to-olefins catalysis. *J. Catal.* **2017**, *345*, 11–23.
- (6) Cao, K.; Fan, D.; Zeng, S.; Fan, B.; Chen, N.; Gao, M.; Zhu, D.; Wang, L.; Tian, P.; Liu, Z. Organic-free synthesis of MOR nanoassemblies with excellent DME carbonylation performance. *Chin. J. Catal.* **2021**, *42*, 1468–1477.
- (7) Liu, Z. Q.; Yi, X. F.; Wang, G. R.; Tang, X. M.; Li, G. C.; Huang, L.; Zheng, A. M. Roles of 8-ring and 12-ring channels in mordenite for carbonylation reaction: From the perspective of molecular adsorption and diffusion. *J. Catal.* **2019**, *369*, 335–344.
- (8) Guo, Z.; Li, X.; Hu, S.; Ye, G.; Zhou, X.; Coppens, M. O. Understanding the Role of Internal Diffusion Barriers in Pt/Beta Zeolite Catalyzed Isomerization of n-Heptane. *Angew. Chem., Int. Ed.* **2020**, *59*, 1548–1551.
- (9) Karwacki, L.; Kox, M. H. F.; de Winter, D. A. M.; Drury, M. R.; Meeldijk, J. D.; Stavitski, E.; Schmidt, W.; Mertens, M.; Cubillas, P.; John, N.; Chan, A.; Kahn, N.; Bare, S. R.; Anderson, M.; Kornatowski, J.; Weckhuysen, B. M. Morphology-dependent zeolite intergrowth structures leading to distinct internal and outer-surface molecular diffusion barriers. *Nat. Mater.* **2009**, *8*, 959–965.
- (10) Aramburo, L. R.; Ruiz-Martinez, J.; Hofmann, J. P.; Weckhuysen, B. M. Imaging the effect of a hydrothermal treatment on the pore accessibility and acidity of large ZSM-5 zeolite crystals by selective staining. *Catal. Sci. Technol.* **2013**, *3*, 1208–1214.
- (11) Ye, G.; Sun, Y.; Guo, Z.; Zhu, K.; Liu, H.; Zhou, X.; Coppens, M.-O. Effects of zeolite particle size and internal grain boundaries on Pt/Beta catalyzed isomerization of n-pentane. *J. Catal.* **2018**, *360*, 152–159.
- (12) Saint Remi, J. C.; Lauerer, A.; Chmelik, C.; Vandendael, I.; Terryn, H.; Baron, G. V.; Denayer, J. F. M.; Koerger, J. The role of crystal diversity in understanding mass transfer in nanoporous materials. *Nat. Mater.* **2016**, *15*, 401–406.
- (13) Chen, L.-H.; Li, Y.; Su, B.-L. Hierarchy in materials for maximized efficiency. *Natl. Sci. Rev.* **2020**, *7*, 1626–1630.
- (14) Hedlund, J.; Nobandegani, M. S.; Yu, L. The origin of the surface barrier in nanoporous materials. *J. Membr. Sci.* **2022**, *641*, 119893.
- (15) Ye, G.; Guo, Z.; Sun, Y.; Zhu, K.; Liu, H.; Zhou, X.; Coppens, M.-O. Probing the Nature of Surface Barriers on ZSM-5 by Surface Modification. *Chem. Ing. Tech.* **2017**, *89*, 1333–1342.


- (16) Peng, S.; Gao, M.; Li, H.; Yang, M.; Ye, M.; Liu, Z. Control of surface barriers in mass transfer to modulate methanol-to-olefins reaction over SAPO-34 zeolites. *Angew. Chem., Int. Ed.* **2020**, *59*, 21945–21948.
- (17) Gao, M.; Li, H.; Yang, M.; Gao, S.; Wu, P.; Tian, P.; Xu, S.; Ye, M.; Liu, Z. Direct quantification of surface barriers for mass transfer in nanoporous crystalline materials. *Commun. Chem.* **2019**, *2*, 43.
- (18) Hu, S.; Liu, J.; Ye, G.; Zhou, X.; Coppens, M.-O.; Yuan, W. Effect of External Surface Diffusion Barriers on Platinum/Beta-Catalyzed Isomerization of n-Pentane. *Angew. Chem., Int. Ed.* **2021**, *60*, 14394.
- (19) Jiao, F.; Pan, X.; Gong, K.; Chen, Y.; Li, G.; Bao, X. Shape-Selective Zeolites Promote Ethylene Formation from Syngas via a Ketene Intermediate. *Angew. Chem., Int. Ed.* **2018**, *57*, 4692–4696.
- (20) Cheung, P.; Bhan, A.; Sunley, G. J.; Iglesia, E. Selective carbonylation of dimethyl ether to methyl acetate catalyzed by acidic zeolites. *Angew. Chem., Int. Ed.* **2006**, *45*, 1617–1620.
- (21) He, T.; Hou, G. J.; Li, J. J.; Liu, X. C.; Xu, S. T.; Han, X. W.; Bao, X. H. Highly selective methanol-to-olefin reaction on pyridine modified H-mordenite. *J. Energy Chem.* **2017**, *26*, 354–358.
- (22) Wang, Y.; Zhou, W.; Kang, J.; Cheng, K.; He, S.; Shi, J.; Zhou, C.; Zhang, Q.; Chen, J.; Peng, L.; Chen, M. Direct Conversion of Syngas into Methyl Acetate, Ethanol and Ethylene by Relay Catalysis via Dimethyl Ether Intermediate. *Angew. Chem., Int. Ed.* **2018**, *57*, 12012–12016.
- (23) Chen, W.; Li, G.; Yi, X.; Day, S. J.; Tarach, K. A.; Liu, Z.; Liu, S.-B.; Tsang, S. C. E.; Gora-Marek, K.; Zheng, A. Molecular Understanding of the Catalytic Consequence of Ketene Intermediates under Confinement. *J. Am. Chem. Soc.* **2021**, *143*, 15440–15452.
- (24) Grad, P. *Debut of a Coal-to-ethanol Plant*; <https://www.chemengonline.com/debut-coal-ethanol-plant/>.
- (25) Liu, Z. Q.; Yi, X. F.; Wang, G. R.; Tang, X. M.; Li, G. C.; Huang, L.; Zheng, A. M. Roles of 8-ring and 12-ring channels in mordenite for carbonylation reaction: From the perspective of molecular adsorption and diffusion. *J. Catal.* **2019**, *369*, 335–344.
- (26) Bhan, A.; Allian, A. D.; Sunley, G. J.; Law, D. J.; Iglesia, E. Specificity of sites within eight-membered ring zeolite channels for carbonylation of methyls to acetyls. *J. Am. Chem. Soc.* **2007**, *129*, 4919–4924.
- (27) Boronat, M.; Martinez-Sanchez, C.; Law, D.; Corma, A. Enzyme-like Specificity in Zeolites: A Unique Site Position in Mordenite for Selective Carbonylation of Methanol and Dimethyl Ether with CO. *J. Am. Chem. Soc.* **2008**, *130*, 16316–16323.
- (28) Liu, J.; Xue, H.; Huang, X.; Wu, P.-H.; Huang, S.-J.; Liu, S.-B.; Shen, W. Stability Enhancement of H-Mordenite in Dimethyl Ether Carbonylation to Methyl Acetate by Pre-adsorption of Pyridine. *Chin. J. Catal.* **2010**, *31*, 729–738.
- (29) Reule, A. A. C.; Sawada, J. A.; Semagina, N. Effect of selective 4-membered ring dealumination on mordenite-catalyzed dimethyl ether carbonylation. *J. Catal.* **2017**, *349*, 98–109.
- (30) Wang, X.; Li, R.; Yu, C.; Liu, Y.; Zhang, L.; Xu, C.; Zhou, H. Enhancing the dimethyl ether carbonylation performance over mordenite catalysts by simple alkaline treatment. *Fuel* **2019**, *239*, 794–803.
- (31) Bai, L. Y.; Xiong, Z. P.; Zhan, E. S.; Li, S.; Shen, W. J. Piperazine as a versatile organic structure-directing agent for zeolite synthesis: effect of SiO₂/Al₂O₃ ratio on phase selectivity. *J. Mater. Sci.* **2019**, *54*, 7589–7602.
- (32) Lu, K.; Huang, J.; Ren, L.; Li, C.; Guan, Y.; Hu, B.; Xu, H.; Jiang, J.; Ma, Y.; Wu, P. High Ethylene Selectivity in Methanol-to-Olefin (MTO) Reaction over MOR-Zeolite Nanosheets. *Angew. Chem., Int. Ed.* **2020**, *59*, 6258–6262.
- (33) Ma, M.; Huang, X.; Zhan, E.; Zhou, Y.; Xue, H.; Shen, W. Synthesis of mordenite nanosheets with shortened channel lengths and enhanced catalytic activity. *J. Mater. Chem. A* **2017**, *5*, 8887–8891.
- (34) Yuan, Y.; Wang, L.; Liu, H.; Tian, P.; Yang, M.; Xu, S.; Liu, Z. Facile preparation of nanocrystal-assembled hierarchical mordenite zeolites with remarkable catalytic performance. *Chin. J. Catal.* **2015**, *36*, 1910–1919.
- (35) Kumar, M.; Berkson, Z. J.; Clark, R. J.; Shen, Y.; Prisco, N. A.; Zheng, Q.; Zeng, Z.; Zheng, H.; McCusker, L. B.; Palmer, J. C.; Chmelka, B. F.; Rimer, J. D. Crystallization of Mordenite Platelets using Cooperative Organic Structure-Directing Agents. *J. Am. Chem. Soc.* **2019**, *141*, 20155–20165.
- (36) Li, L.; Wang, Q.; Liu, H.; Sun, T.; Fan, D.; Yang, M.; Tian, P.; Liu, Z. Preparation of Spherical Mordenite Zeolite Assemblies with Excellent Catalytic Performance for Dimethyl Ether Carbonylation. *ACS Appl. Mater. Interfaces* **2018**, *10*, 32239–32246.
- (37) Dedecek, J.; Wichterlova, B. Co²⁺ ion siting in pentasil-containing zeolites. I. Co²⁺ ion sites and their occupation in mordenite. A Vis-NIR diffuse reflectance spectroscopy study. *J. Phys. Chem. B* **1999**, *103*, 1462–1476.
- (38) Janda, A.; Bell, A. T. Effects of Si/Al Ratio on the Distribution of Framework Al and on the Rates of Alkane Monomolecular Cracking and Dehydrogenation in H-MFI. *J. Am. Chem. Soc.* **2013**, *135*, 19193–19207.
- (39) Zholobenko, V. L.; Makarova, M. A.; Dwyer, J. INHOMOGENEITY OF BRONSTED ACID SITES IN H-MORDENITE. *J. Phys. Chem.* **1993**, *97*, 5962–5964.
- (40) Wakabayashi, F.; Kondo, J.; Wada, A.; Domen, K.; Hirose, C. FT-IR Studies of the Interaction Between Zeolitic Hydroxyl-groups and Small Molecules 0.1. Adsorption of Nitrogen on H-mordenite at Low-temperature. *J. Phys. Chem.* **1993**, *97*, 10761–10768.
- (41) Rasmussen, D. B.; Christensen, J. M.; Temel, B.; Studt, F.; Moses, P. G.; Rossmeisl, J.; Riisager, A.; Jensen, A. D. Reaction mechanism of dimethyl ether carbonylation to methyl acetate over mordenite a combined DFT/experimental study. *Catal. Sci. Technol.* **2017**, *7*, 1141–1152.
- (42) Li, Y.; Sun, Q.; Huang, S. Y.; Cheng, Z. Z.; Cai, K.; Lv, J.; Ma, X. B. Dimethyl ether carbonylation over pyridine-modified MOR: Enhanced stability influenced by acidity. *Catal. Today* **2018**, *311*, 81–88.
- (43) Jin, D.; Ye, G.; Zheng, J.; Yang, W.; Zhu, K.; Coppens, M. O.; Zhou, X. Hierarchical Silicoaluminophosphate Catalysts with Enhanced Hydroisomerization Selectivity by Directing the Orientated Assembly of Premanufactured Building Blocks. *ACS Catal.* **2017**, *7*, 5887–5902.
- (44) Wu, P.; Yang, M.; Sun, L.; Zeng, S.; Xu, S.; Tian, P.; Liu, Z. Synthesis of nanosized SAPO-34 with the assistance of bifunctional amine and seeds. *Chem. Commun.* **2018**, *54*, 11160–11163.
- (45) Yue, T.; Liu, W.; Li, L.; Zhao, X.; Zhu, K.; Zhou, X.; Yang, W. Crystallization of ATO silicoaluminophosphates nanocrystalline spheroids using a phase-transfer synthetic strategy for n-heptane hydroisomerization. *J. Catal.* **2018**, *364*, 308–327.
- (46) Wloch, J. Effect of surface etching of ZSM-5 zeolite crystals on the rate of n-hexane sorption. *Microporous Mesoporous Mater.* **2003**, *62*, 81–86.
- (47) Kortunov, P.; Vasenkov, S.; Chmelik, C.; Karger, J.; Ruthven, D. M.; Wloch, J. Influence of defects on the external crystal surface on molecular uptake into MFI-type zeolites. *Chem. Mater.* **2004**, *16*, 3552–3558.
- (48) Jelfs, K. E.; Slater, B.; Lewis, D. W.; Willock, D. J. In The role of organic templates in controlling zeolite crystal morphology. *Stud. Surf. Sci. Catal.* **2007**, *170B*, 1685–1692.
- (49) Li, F.; Yang, L.; Xu, G.; Huang, X.; Yang, X.; Wei, X.; Ren, Z.; Shen, G.; Han, G. Hydrothermal self-assembly of hierarchical flower-like ZnO nanospheres with nanosheets and their application in Li-ion batteries. *J. Alloys Compd.* **2013**, *577*, 663–668.
- (50) Gao, B.; Tian, P.; Li, M.; Yang, M.; Qiao, Y.; Wang, L.; Xu, S.; Liu, Z. In situ growth and assembly of microporous aluminophosphate nanosheets into ordered architectures at low temperature and their enhanced catalytic performance. *J. Mater. Chem. A* **2015**, *3* (15), 7741–7749.
- (51) Cundy, C. S.; Cox, P. A. The hydrothermal synthesis of zeolites: Precursors, intermediates and reaction mechanism. *Microporous Mesoporous Mater.* **2005**, *82* (1–2), 1–78.

(52) Ghosh Chaudhuri, R.; Paria, S. Core/Shell Nanoparticles: Classes, Properties, Synthesis Mechanisms, Characterization, and Applications. *Chem. Rev.* **2012**, *112* (4), 2373–2433.


(53) Ahn, S. H.; Lee, H.; Hong, S. B. Crystallization Mechanism of Cage-Based, Small-Pore Molecular Sieves: A Case Study of CHA and LEV Structures. *Chem. Mater.* **2017**, *29* (13), 5583–5590.




JACS Au
AN OPEN ACCESS JOURNAL OF THE AMERICAN CHEMICAL SOCIETY



Editor-in-Chief
Prof. Christopher W. Jones
Georgia Institute of Technology, USA

Open for Submissions 

pubs.acs.org/jacsau  ACS Publications
Most Trusted. Most Cited. Most Read.